

ON THE EFFECT OF REFLECTANCE ON PHASOR FIELD NON-LINE-OF-SIGHT IMAGING

Ibón Guillén^{1*}

Xiaochun Liu²

Andreas Velten^{2,3}

Diego Gutierrez¹

Adrian Jarabo¹

¹Graphics and Imaging Lab, Universidad de Zaragoza - I3A

²Department of Electrical and Computer Engineering, University of Wisconsin Madison

³Department of Biostatistics and Medical Informatics, University of Wisconsin Madison

ABSTRACT

Non-line-of-sight (NLOS) imaging aims to visualize occluded scenes by exploiting indirect reflections on visible surfaces. Previous methods approach this problem by inverting the light transport on the hidden scene, but are limited to isolated, diffuse objects. The recently introduced phasor fields framework computationally poses NLOS reconstruction as a virtual line-of-sight (LOS) problem, lifting most assumptions about the hidden scene. In this work we complement recent theoretical analysis of phasor field-based reconstruction, by empirically analyzing the effect of reflectance of the hidden scenes on reconstruction. We experimentally study the reconstruction of hidden scenes composed of objects with increasingly specular materials. Then, we evaluate the effect of the virtual aperture size on the reconstruction, and establish connections between the effect of these two different dimensions on the results. We hope our analysis helps to characterize the imaging capabilities of this promising new framework, and foster new NLOS imaging modalities.

Index Terms— Phasor Fields, BRDFs, NLOS imaging

1. INTRODUCTION

Non-line-of-sight (NLOS) imaging techniques aim to recover scenes that are occluded or out of the line of sight of the observer, by leveraging indirect reflections on secondary diffuse surfaces. Most NLOS imaging techniques use ultrashort pulsed light sources and ultrafast imaging devices [1]. Transient imaging systems [2] are able to resolve the time-of-flight of light in the order of nano- and pico-seconds. This allows to computationally invert the light transport for recovering the hidden geometry [3–9]. Unfortunately, these approaches are based on inverting a simple approximate light transport model, imposing several assumptions including three-bounce illumination, no occlusions (with the notable exception of [10]), and diffuse reflectance. This last assumption is crucial, since specularities introduce light transport asymmetries, significantly complicating inversion.

Recently, Liu et al. [11] introduced *phasor fields*, a computational approach that posed NLOS imaging as a virtual

line-of-sight (LOS) problem. The key idea is that by leveraging the captured time-of-flight light information, a virtual wave field can be propagated in the same way as light does. This allows to transform the diffuse secondary wall (the relay wall) into a virtual camera. Therefore, the inversion problem is posed as the forward imaging process of a regular LOS camera, which does not suffer from limitations imposed by inverting a light transport model. It naturally deals with scenes of arbitrary complexity, including occlusions, clutter, multiple scattering, or specular reflectance, in the same way as conventional cameras do. Lastly, phasor field imaging is oblivious to the underlying transient capture method as long as the visible relay surface can be assumed to be planar.

In this work, we systematically analyze the effect of reflectance on phasor fields-based NLOS imaging. We provide experimental examples of NLOS reconstruction of scenes with different levels of material complexity. In particular, we explore the effect of the bidirectional reflectance distribution function (BRDF), that models how a surface reflects light, on reconstruction using phasor fields. For that, we analyze reconstructions for objects with different geometric complexity, with materials with increasing level of specularity. Then, following Liu et al. [12], we explore the effect of the size of the virtual aperture on the reconstruction, and how that affects the amount of radiance reaching the relay wall (the *missing cone problem*). We hope our work can give new experimental insights in this new NLOS imaging modality, which might lead to novel applications on NLOS material recognition.

2. PHASOR FIELDS

Here we briefly review the theory behind phasor fields [11], and its use in NLOS imaging. For a more complete theoretical derivation we refer to the original manuscript, or the work by Reza et al. [13].

Let us define a phasor $\mathcal{P}(\mathbf{x}, t)$ as the mean subtracted irradiance [Wm^{-2}] at point \mathbf{x} and time t , as:

$$\mathcal{P}(\mathbf{x}, t) \equiv \frac{1}{\tau} \int_{t-\frac{\tau}{2}}^{t+\frac{\tau}{2}} |\mathcal{E}(\mathbf{x}, t')|^2 dt' - \frac{1}{T} \int_{t-\frac{T}{2}}^{t+\frac{T}{2}} |\mathcal{E}(\mathbf{x}, t')|^2 dt', \quad (1)$$

*Corresponding author: ibon@unizar.es

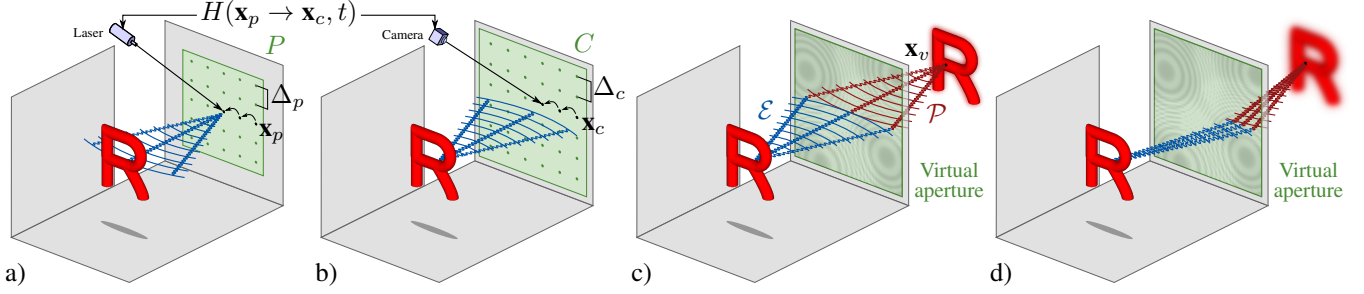


Fig. 1: Scene setting. **a)** A pulsed light emitter sequentially illuminates a relay surface P and **b)** the light reflected back is collected by a transient capture device focusing at a visible surface C (not necessarily the same surface). The resulting impulse response $H(\mathbf{x}_p \rightarrow \mathbf{x}_c, t)$ encodes the time-resolved 5D light transport in the hidden scene. **Scene reconstruction.** The original irradiance signal $|\mathcal{E}|^2$ captured at C is computationally encoded into a virtual wave field (the *phasor field*) \mathcal{P} . This phasor field is computationally focused to image the hidden scene, using the relay surface as a virtual aperture. When the objects in the hidden scene are perfectly diffuse **c)** they reflect light back to the entire virtual aperture. On the other hand, increasingly specular surfaces **d)** reflect the field towards specific directions of the aperture; this results into a loss of spatial resolution except for very dense sampling rate on the relay wall.

where $\mathcal{E}(\mathbf{x}, t)$ [$\sqrt{\text{Wm}^{-2}}$] is a quasi-monochromatic scalar field incident on (or reflected from) a surface, τ represents the averaging of the intensity at a fast detector, and the second integral is a long-term average intensity over an interval $T \gg \tau$ of the signal as seen by a conventional photodetector.

Making use of an ultra short pulsed light emitter, we illuminate a series of points \mathbf{x}_p over a relay surface P , and collect the returning light from each pulse with an ultrafast imaging device focusing at a set of points \mathbf{x}_c over a visible surface C , as illustrated in Figure 1(a-b). The captured data results on the impulse response function $H(\mathbf{x}_p \rightarrow \mathbf{x}_c, t)$ of the scene. Leveraging the fact that the light transport is linear in space and time-invariant [14, 15], we can use H to compute the propagation of a phasor field \mathcal{P} over the hidden scene as

$$\mathcal{P}(\mathbf{x}_c, t) = \int_P \int_{-\infty}^{+\infty} \mathcal{P}(\mathbf{x}_p, t - \tau) H(\mathbf{x}_p \rightarrow \mathbf{x}_c, t) d\tau d\mathbf{x}_p \quad (2)$$

where $\mathcal{P}(\mathbf{x}_p, t)$ is the emitted *phasor field*, a virtual complex field whose amplitude and phase are set computationally. Note that the parameters of the field are bounded by validity conditions under which the method produces best results [11, 13, 16].

Once we obtain the field $\mathcal{P}(\mathbf{x}_c, t)$ on the visible surface C , we computationally propagate it by solving the Rayleigh–Sommerfeld diffraction (RSD) integral [17]. The main consequence is that we apply to our captured data any virtual photography system with aperture at C , by characterizing its image formation function $\Phi(\cdot)$. The computational field can be then imaged at a point \mathbf{x}_v by

$$I(\mathbf{x}_v) = \Phi(\mathcal{P}(\mathbf{x}_c, t)). \quad (3)$$

In this work we use a (virtual) confocal time-gated camera, which allows us to recover both irradiance and depth information (see [11] for details). The reconstructions are generated by directly solving the discrete RSD. Alternative

virtual photography systems and solvers can be found elsewhere [7, 11, 18].

3. NON-DIFFUSE SURFACES IN PHASOR FIELDS

The RSD propagator (Equation (3)) requires that the source plane S to be diffuse. The camera we use bases primarily on RSD propagators from the aperture of the relay wall to a virtual sensor. On the other hand, light transport in the NLOS scene, including arbitrary reflectances, is fully characterized by the impulse response function $H(\mathbf{x}_p \rightarrow \mathbf{x}_c, t)$. Therefore, the diffuse constraint only applies to the relay wall. Rather than reconstructing the geometry and reflectance of the scene, phasor field-based virtual cameras reconstruct phasor field irradiance from the scene towards the virtual aperture as a function of position and time, analogous to their LOS counterparts. The reconstructed signal thus corresponds to the averaged irradiance for the entire aperture. This is illustrated in Figure 1(c-d).

Prior methods seek to reconstruct NLOS geometry, which requires correct modeling of albedo and BRDF, occlusions, and interreflections, resulting in a non-linear inverse problem [10]. In the absence of such data from the hidden scene, these prior methods need to rely on simplifying assumptions, thus limiting the range of scenes that can be reconstructed. The impulse response function $H(\mathbf{x}_p \rightarrow \mathbf{x}_c, t)$ does not make any assumption about the surface properties of the hidden scene. Therefore, as we show in the following the changes in material appearance do not significantly affect reconstructions on irradiance.

4. NON-DIFFUSE RECONSTRUCTIONS

Here we analyze the performance of phasor fields-based NLOS imaging in the presence of non-diffuse materials. For

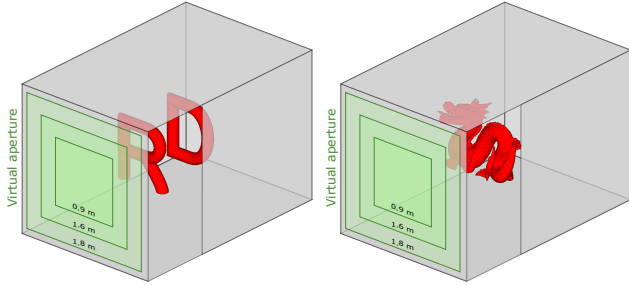


Fig. 2: Overview of the two synthetic scenes used in our work. They feature two occluding letters (**left**) and a dragon statue (**right**). The green areas illustrate the virtual apertures on the relay wall.

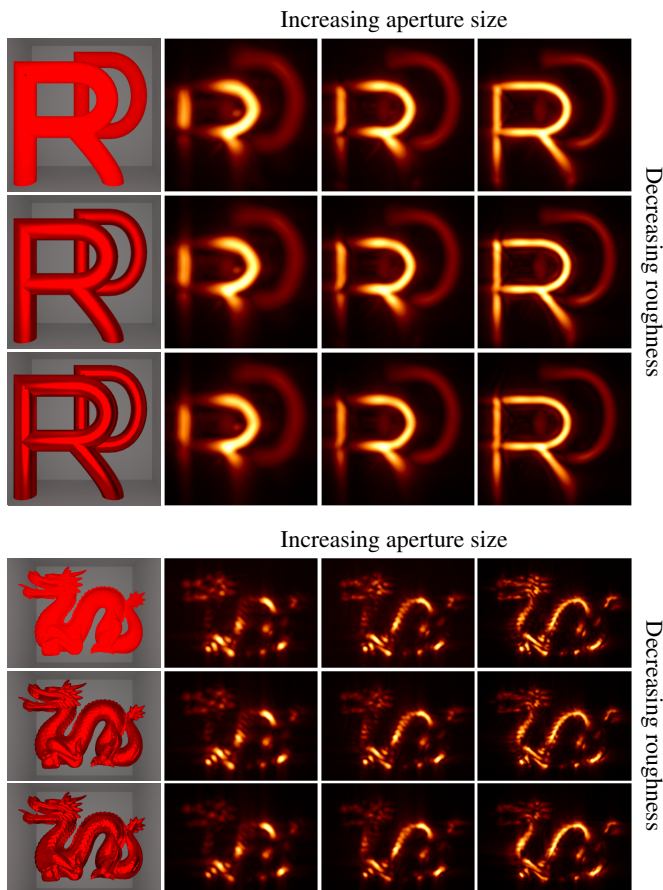


Fig. 3: Irradiance reconstructions, for the letters (**top**) and the dragon statue (**bottom**) scenes. From left to right, render of the scene from the relay wall, and reconstructions for aperture sizes of 0.9 m, 1.6 m and 1.8 m. From top to bottom, increasingly specular targets, with decreasing surface roughness: $\alpha = 1.0$ (perfectly diffuse), $\alpha = 0.4$, and $\alpha = 0.2$.

that, we rely on synthetic scenes with carefully controlled geometry and reflectance.

Scenes description. We use two different scenes, that

consist of a diffuse corridor of $2\text{ m} \times 2\text{ m} \times 3\text{ m}$, with only a single lateral aperture of $1\text{ m} \times 2\text{ m}$ to allow imaging the hidden scene. Inside the corridor we place two different objects of increasing geometric complexity. The first object (Figure 2, left) is a pair of letters (R and D), one partially occluding the other. The letters have rounded shape, and their size is $0.75\text{ m} \times 0.8\text{ m}$. Each letter is placed at 1.25 m and 1.7 m from the relay wall, respectively, and at 0.5 m from the lateral walls of the corridor. The second scene (Figure 2, right), contains a dragon statue of $1.25\text{ m} \times 0.9\text{ m} \times 0.55\text{ m}$, placed at 1.1 m from the relay wall and 0.35 m from the lateral walls. The geometry in this case is of higher complexity, with significant surface detail and self-occlusions. We use the isotropic Ward BRDF [19] for modeling the surface reflectance, with decreasing roughness $\alpha = 1$ (purely diffuse), 0.4 and 0.2 (highly specular surface).

In both scenes the virtual aperture at the relay wall has a size of $1.792\text{ m} \times 1.792\text{ m}$. The relay wall is sampled using 64×64 laser points for the letters scene, and 128×128 laser points for the dragon scene. This gives a laser separation of $\Delta_p = 1.4\text{ cm}$ for the letters scene, and $\Delta_p = 0.7\text{ cm}$ for the dragon statue. We use a single SPAD measurement, at the center of the relay wall.

Simulation. We compute the impulse response function $H(\mathbf{x}_p \rightarrow \mathbf{x}_c, t)$ using an open-source transient renderer [20], including up to five indirect bounces, to maximize multiple scattering. The software has been shown to provide a reasonable match to real measurements [11, 21].

Reconstruction results. We reconstruct both scenes using a conservative phasor field wavelength of $\lambda = 4\Delta_p$. Since we use the confocal virtual camera [11], we reconstruct a full 3D volume, with voxel size $\Delta_x = 4\Delta_p$. Figure 3 (top) shows the resulting irradiance reconstructions from the letters scene, while Figure 3 (bottom) shows reconstruction for the dragon scene. Along the y-axis we increase the specularity (see leftmost row for a depiction of what a conventional camera would have captured), while on the x-axis we vary the size of the aperture at the relay wall. It can be seen that the surfaces facing the relay wall are accurately reconstructed, even at the highest specular level, while those facing outwards are mostly missing from the reconstructions, due to limitations on the recovered frequencies [12]. Interestingly, we can see that as we decrease the aperture at the relay wall, the resolution of the image and thus the recovered detail is significantly reduced. This is in part due the decreasing amount of signal reflected back to the aperture, as exemplified in Figure 1. This is specially visible in the dragon scene, where most of the geometric details are blurred out.

Error analysis. Similar to previous related work [8, 11], we numerically evaluate the quality of the reconstructions by measuring the reconstruction error in depth from the relay wall. We compute a voxelization of the synthetic geometry, and take the first visible surface as the ground truth. Then, we threshold our 3D reconstruction, and select the maximum

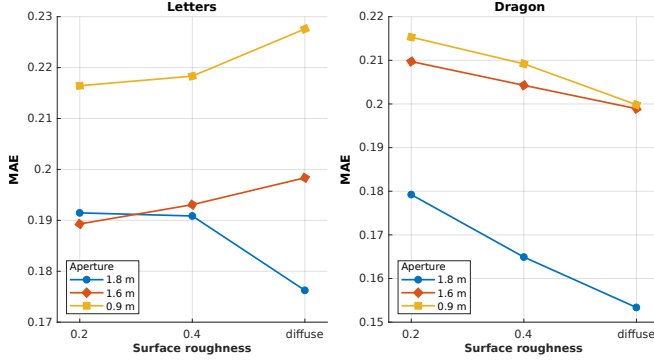


Fig. 4: Mean Absolute Error (in meters), from the letters (left) and the dragon statue (right) scenes, as a function of surface roughness, for fixed aperture sizes.

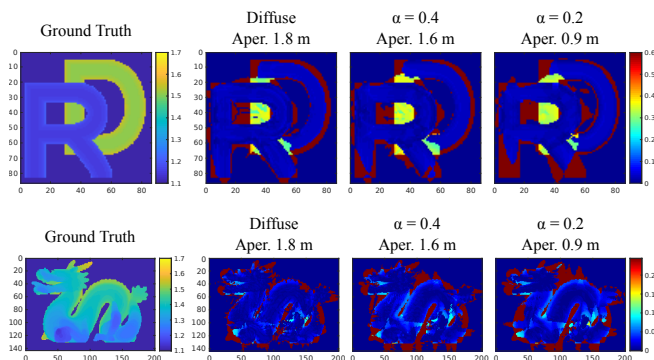


Fig. 5: Recovered depth reconstruction error, for the letters (top) and the dragon statue (bottom) scenes. For each scene, from left to right, depth map of the voxelized scene geometry (ground truth), and error maps of the recovered depth compared with the ground truth, for the perfectly diffuse with 1.8^2 m^2 aperture, roughness 0.4 with 1.6^2 m^2 aperture, and roughness 0.2 with 0.9^2 m^2 aperture variants of each scene. At the right of each depth map and error series are the corresponding color scales, in meters.

along the line perpendicular to the relay wall as the reconstructed geometry. The mean absolute error (MAE) of the reconstruction of each scene, for each level of specularity, are shown in Figure 4. For each pair of aperture size and specularly level we use the best possible thresholding for the MAE metric. Additionally, Figure 5 shows error maps of the distribution of the error across the reconstructed depth map.

As expected, the reconstructed depth is more accurate when a bigger aperture is used to image the hidden scene. Also, since diffuse surfaces reflect light more evenly, and therefore are more likely to reflect light towards the virtual aperture, we in general obtain slightly better reconstructions, although that does not hold for simple scenes high specularities lead to less scattered light, and therefore to more signal reflected towards the aperture. To illustrate this behavior,

in Figure 5 we show the results from the theoretically best reconstruction (biggest aperture of 1.8^2 m^2 , diffuse surfaces) compared to the worst setting (small aperture of 0.9^2 m^2 , almost perfect specular surfaces). Finally, it is interesting to note that, similarly to the irradiance maps shown in Figure 3, slanted surfaces are missing from the reconstruction, since their normals lie outside the aperture and cannot be recovered.

5. CONCLUSIONS AND FUTURE WORK

In this work we have analyzed the effect of the BRDF in the occluded geometry for NLOS imaging using phasor fields. We have provided empirical evidence that the phasor field method can robustly image NLOS scenes with arbitrary reflectances. As described in the theoretical derivations of phasor fields [11, 13, 22] and observed in experimental validation [23], the reason is that the phasor field propagates independently from the BRDF of the carrier. However, as in conventional cameras, if the reflected light does not propagate towards the aperture it cannot be imaged.

In order to evaluate this effect, we have additionally analyzed how the size of the aperture affects the reconstruction. As expected, as the aperture size decreases, the probability of a surface reflecting towards the aperture decreases, specially in the case of specular surfaces. Consequently, as the aperture size decreases, the virtual depth of field decreases too, and surfaces oriented towards the aperture appear sharper in the reconstruction.

Our work gives empirical evidence on the potential of phasor fields to image arbitrary NLOS scenes, focusing on one of the key limitations of previous work that assumed diffuse reflectance. We hope it will give insights on the capabilities and limitations of this promising theoretical framework. Also, our analysis suggests that the reflectance of the carrier is encoded in the propagated phasor field. As illustrated in the Figure 1(d), specular surfaces have a different angular amplitude response than diffuse ones. As a future work, we would like to analyze such amplitude responses, potentially for capturing reflectances in complex NLOS scenes.

Acknowledgments

This work was funded by DARPA through the DARPA REVEAL project (HR0011-16-C-0025), the European Research Council (ERC) under the EU's Horizon 2020 research and innovation programme (project CHAMELEON, grant no. 682080), the Spanish Ministerio de Economía y Competitividad (project TIN2016-78753-P) the BBVA Foundation through a Leonardo Grant, the NASA Innovative Advanced Concepts (NIAC) Program (NNX15AQ29G), the Air Force Office of Scientific Research (AFOSR) Young Investigator Program (FA9550-15-1-0208), and the Office of Naval Research (ONR, N00014-15-1-2652).

6. REFERENCES

- [1] Adrian Jarabo, Belen Masia, Julio Marco, and Diego Gutierrez, "Recent advances in transient imaging: A computer graphics and vision perspective," *Visual Informatics*, vol. 1, no. 1, 2017.
- [2] Andreas Velten, Di Wu, Adrian Jarabo, Belen Masia, Christopher Barsi, Chinmaya Joshi, Everett Lawson, Mounqi G. Bawendi, Diego Gutierrez, and Ramesh Raskar, "Femto-photography: Capturing and visualizing the propagation of light," *ACM Transactions on Graphics*, vol. 32, no. 4, 2013.
- [3] Ahmed Kirmani, Tyler Hutchison, James Davis, and Ramesh Raskar, "Looking around the corner using ultrafast transient imaging," *International Journal of Computer Vision*, vol. 95, no. 1, 2011.
- [4] Andreas Velten, Thomas Willwacher, Otkrist Gupta, Ashok Veeraraghavan, Mounqi G Bawendi, and Ramesh Raskar, "Recovering three-dimensional shape around a corner using ultrafast time-of-flight imaging," *Nature Communications*, vol. 3, 2012.
- [5] Otkrist Gupta, Thomas Willwacher, Andreas Velten, Ashok Veeraraghavan, and Ramesh Raskar, "Reconstruction of hidden 3d shapes using diffuse reflections," *Optics Express*, vol. 20, no. 17, 2012.
- [6] Mauro Buttafava, Jessica Zeman, Alberto Tosi, Kevin Eliceiri, and Andreas Velten, "Non-line-of-sight imaging using a time-gated single photon avalanche diode," *Optics Express*, vol. 23, no. 16, 2015.
- [7] Victor Arellano, Diego Gutierrez, and Adrian Jarabo, "Fast back-projection for non-line of sight reconstruction," *Optics Express*, vol. 25, no. 10, 2017.
- [8] Matthew O'Toole, David B. Lindell, and Gordon Wetzstein, "Confocal non-line-of-sight imaging based on the light-cone transform," *Nature*, vol. 555, 2018.
- [9] Shumian Xin, Sotiris Nousias, Kiriakos N. Kutulakos, Aswin C. Sankaranarayanan, Srinivasa G. Narasimhan, and Ioannis Gkioulekas, "A theory of fermat paths for non-line-of-sight shape reconstruction," in *Proceedings of IEEE/CVF Conference on Computer Vision and Pattern Recognition*, 2019.
- [10] Felix Heide, Matthew O'Toole, Kai Zang, David B Lindell, Steven Diamond, and Gordon Wetzstein, "Non-line-of-sight imaging with partial occluders and surface normals," *ACM Transactions on Graphics*, vol. 38, no. 3, 2019.
- [11] Xiaochun Liu, Ibón Guillén, Marco La Manna, Ji Hyun Nam, Syed Azer Reza, Toan Huu Le, Diego Gutierrez, Adrian Jarabo, and Andreas Velten, "Non-line-of-sight imaging using phasor-field virtual wave optics," *Nature*, vol. 572, 2019.
- [12] Xiaochun Liu, Sebastian Bauer, and Andreas Velten, "Analysis of feature visibility in non-line-of-sight measurements," in *Proceedings of IEEE/CVF Conference on Computer Vision and Pattern Recognition*, 2019.
- [13] Syed Azer Reza, Marco La Manna, Sebastian Bauer, and Andreas Velten, "Phasor field waves: A Huygens-like light transport model for non-line-of-sight imaging applications," *Optics Express*, vol. 27, no. 20, 2019.
- [14] Pradeep Sen, Billy Chen, Gaurav Garg, Stephen R. Marschner, Mark Horowitz, Marc Levoy, and Hendrik Lensch, "Dual photography," *ACM Transactions on Graphics*, vol. 24, no. 3, 2005.
- [15] Matthew O'Toole, Felix Heide, Lei Xiao, Matthias B Hullin, Wolfgang Heidrich, and Kiriakos N Kutulakos, "Temporal frequency probing for 5d transient analysis of global light transport," *ACM Transactions on Graphics*, vol. 33, no. 4, 2014.
- [16] Jeremy A. Teichman, "Phasor field waves: a mathematical treatment," *Optics Express*, vol. 27, no. 20, 2019.
- [17] Arnold Sommerfeld, *Lectures on theoretical physics: Optics*, vol. 4, Academic press, 1954.
- [18] David B. Lindell, Gordon Wetzstein, and Matthew O'Toole, "Wave-based non-line-of-sight imaging using fast f-k migration," *ACM Transactions on Graphics*, vol. 38, no. 4, 2019.
- [19] Gregory J. Ward, "Measuring and modeling anisotropic reflection," *ACM SIGGRAPH Computer Graphics*, vol. 26, no. 2, 1992.
- [20] Adrian Jarabo, Julio Marco, Adolfo Muñoz, Raul Buisan, Wojciech Jarosz, and Diego Gutierrez, "A framework for transient rendering," *ACM Transactions on Graphics*, vol. 33, no. 6, 2014.
- [21] Julio Marco, Quercus Hernandez, Adolfo Muñoz, Yue Dong, Adrian Jarabo, Min Kim, Xin Tong, and Diego Gutierrez, "Deeptof: Off-the-shelf real-time correction of multipath interference in time-of-flight imaging," *ACM Transactions on Graphics*, vol. 36, no. 6, 2017.
- [22] Justin Dove and Jeffrey H. Shapiro, "Paraxial theory of phasor-field imaging," *Optics Express*, vol. 27, no. 13, 2019.
- [23] Syed Azer Reza, Marco La Manna, Sebastian Bauer, and Andreas Velten, "Phasor field waves: experimental demonstrations of wave-like properties," *Optics Express*, vol. 27, no. 22, 2019.